Supporting Information

Zwitterionic near-infrared fluorophore-conjugated epidermal growth factor for fast, real-time, and target cell-specific cancer imaging

Hyunjin Kim[a], Mi Hyeon Cho[a], Hak Soo Choi[b], Byung Il Lee[a], Yongdoo Choi [a,*]

[a]Research Institute, National Cancer Center, 323 Ilsan-ro, Goyang, Gyeonggi 10408, Republic of Korea

[b]Gordon Center for Medical Imaging, Department of Radiology, Massachusetts General Hospital and Harvard Medical School, Boston, MA 02114, USA.

[*]Corresponding author:
Yongdoo Choi, Ph.D.
Tel: +82-31-920-2512
E-mail: ydchoi@ncc.re.kr

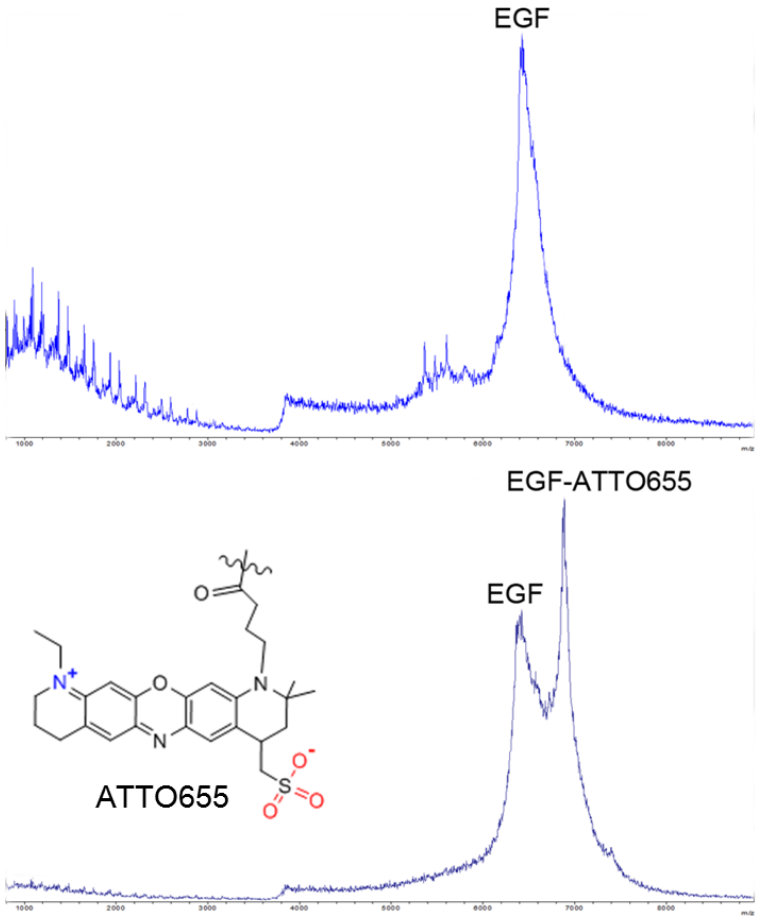

Figure S1. Comparison of the mass spectra of EGF and EGF-ATTO655 using MALDI-TOF. Inset image: chemical structure of the conjugated ATTO655 dye.

Analysis of the dye conjugation site

Precipitation and in-solution digestion

EGF and EGF-ATTO655 were precipitated using cold acetone, reduced by 10 mM DTT, and alkylated by idoacetamide (IAA). The alkylated samples were digested with mass spectrometry-grade Glu-C endoprotease in 25 mM ammonium carbonate (NH_4CO_3) for 12 h at 37 °C. Digested peptides were evaporated using a vacuum concentrator and cleaned up using C18 ZipTip (Millipore) for mass spectrometry (MS) analysis.

Liquid chromatography tandem mass spectrometry (LC-MS/MS) analysis

The peptides were analyzed by a Q Exactive™ hybrid quadrupole-orbitrap mass spectrometer (Thermo Fisher Scientific) coupled with an Ultimate 3000 RSLC nano system (Thermo Fisher Scientific). The peptides were loaded onto a trap column (100 μm × 2 cm) packed with Acclaim PepMap100 C18 resin and eluted with a linear gradient from 2% to 35% of solvent B (0.1% formic acid in acetonitrile) for 110 min at a flow rate 300 nL/min. The eluted peptides, separated by the analytical column (EASY-Spray column, 75 μm × 15 cm, Thermo Fisher Scientific), were sprayed into nano-electrospray ionization (ESI) source at an electrospray voltage of 2.1 kV. The Q Exactive Orbitrap mass analyzer was operated in a top 10 data-dependent method. Full MS scans were acquired over the range m/z 300-2,000 with a mass resolution of 70,000 (at m/z 200). The AGC target value was 1.00E+06. The ten most intense peaks with charge state ≥ 2 were fragmented in the higher-energy collisional dissociation (HCD) collision cell with normalized collision energy of 25 and 30, and tandem mass spectra were acquired in the Orbitrap mass analyzer with a mass resolution of 17,500 at m/z 200.

Database search

Database searching of all raw data files was performed in Proteome Discoverer 2.1 software (Thermo Fisher Scientific). SEQUEST-HT was used for database searching against SWISS-PROT human database. Database searching against the corresponding reversed database was also performed to evaluate the false discovery rate (FDR) of peptide identification. The database searching parameters included precursor ion mass tolerance of 10 ppm, fragment ion mass tolerance of 0.08 Da, fixed modification for carbamidomethyl cysteine (+57.021 Da/C), variable modifications for methionine oxidation (+15.995 Da/M), and ATTO655-conjugated lysine (+509.198 Da/K). The FDR of peptide identification was less than 1% at peptide level and extracted with high peptide confidence.

Table S1. Analysis of the fluorescence dye-conjugated site in EGF-ATTO655. Nine fragments were obtained from EGF-ATTO655 digested by Glu-C endoprotease and analyzed by Q Exactive hybrid quadrupole-orbitrap mass spectrometry. A total of 10% and 0.9% of matched sequences were identified in a modified K48 and K28, respectively. Matched mass of b ion and y ion were indicated with red and blue color, respectively.

#1	b^+	b^{2+}	Sequence	y^+	y^{2+}	#2
1	638.30064	319.65396	K28-ATTO655-H_2O			13
2	801.36397	401.18562	Y	1404.59225	702.79976	12
3	872.40108	436.70418	A	1241.52892	621.2681	11
4	1032.43173	516.7195	C-Carbamidomethyl	1170.49181	585.74954	10
5	1146.47466	573.74097	N	1010.46116	505.73422	9
6	1306.50531	653.75629	C-Carbamidomethyl	896.41823	448.71275	8
7	1405.57372	703.2905	V	736.38758	368.69743	7
8	1504.64213	752.82471	V	637.31917	319.16322	6
9	1561.6636	781.33544	G	538.25075	269.62902	5
10	1724.72693	862.8671	Y	481.22929	241.11828	4
11	1837.81099	919.40913	I	318.16596	159.58662	3
12	1894.83245	947.91987	G	205.0819	103.04459	2
13			E	148.06043	74.53386	1

#3	b^+	b^{2+}	Sequence	y^+	y^{2+}	#4
1	157.10839	79.05783	R			11
2	317.13904	159.07316	C-Carbamidomethyl	1992.8771	996.94219	10
3	445.19761	223.10245	Q	1832.84645	916.92686	9
4	608.26094	304.63411	Y	1704.78787	852.89757	8
5	764.36205	382.68466	R	1541.72454	771.36591	7
6	879.389	440.19814	D	1385.62343	693.31535	6
7	992.47306	496.74017	L	1270.59649	635.80188	5
8	1629.76642	815.38685	K48-ATTO655-H_2O	1157.51242	579.25985	4
9	1815.84574	908.42651	W	520.21906	260.61317	3
10	2001.92505	1001.46616	W	334.13975	167.57351	2
11			E	148.06043	74.53386	1

Table S2. Analysis of the fluorescence dye-conjugated site in EGF. EGF was digested with Glu-C endoprotease and analyzed by Q Exactive hybrid quadrupole-orbitrap mass spectrometry. Mass modified with ATTO655 was not indicated for both K28 and K48 from hEGF.

#1	b^+	b^{2+}	Sequence	y^+	y^{2+}	#2
1	129.10224	65.05476	K			13
2	292.16557	146.58642	Y	1404.59225	702.79976	12
3	363.20268	182.10498	A	1241.52892	621.2681	11
4	523.23333	262.1203	C-Carbamidomethyl	1170.49181	585.74954	10
5	637.27626	319.14177	N	1010.46116	505.73422	9
6	797.30691	399.15709	C-Carbamidomethyl	896.41823	448.71275	8
7	896.37532	448.6913	V	736.38758	368.69743	7
8	995.44373	498.22551	V	637.31917	319.16322	6
9	1052.4652	526.73624	G	538.25075	269.62902	5
10	1215.52853	608.2679	Y	481.22929	241.11828	4
11	1328.61259	664.80993	I	318.16596	159.58662	3
12	1385.63405	693.32067	G	205.0819	103.04459	2
13			E	148.06043	74.53386	1

#3	b^+	b^{2+}	Seq.	y^+	y^{2+}	#4
1	157.10839	79.05783	R			11
2	317.13904	159.07316	C-Carbamidomethyl	1483.67870	742.34299	10
3	445.19761	223.10245	Q	1323.64805	662.32766	9
4	608.26094	304.63411	Y	1195.58947	598.29837	8
5	764.36205	382.68466	R	1032.52614	516.76671	7
6	879.38900	440.19814	D	876.42503	438.71615	6
7	992.47306	496.74017	L	761.39809	381.20268	5
8	1120.56802	560.78765	K	648.31402	324.66065	4
9	1306.64734	653.82731	W	520.21906	260.61317	3
10	1492.72665	746.86696	W	334.13975	167.57351	2
11			E	148.06043	74.53386	1

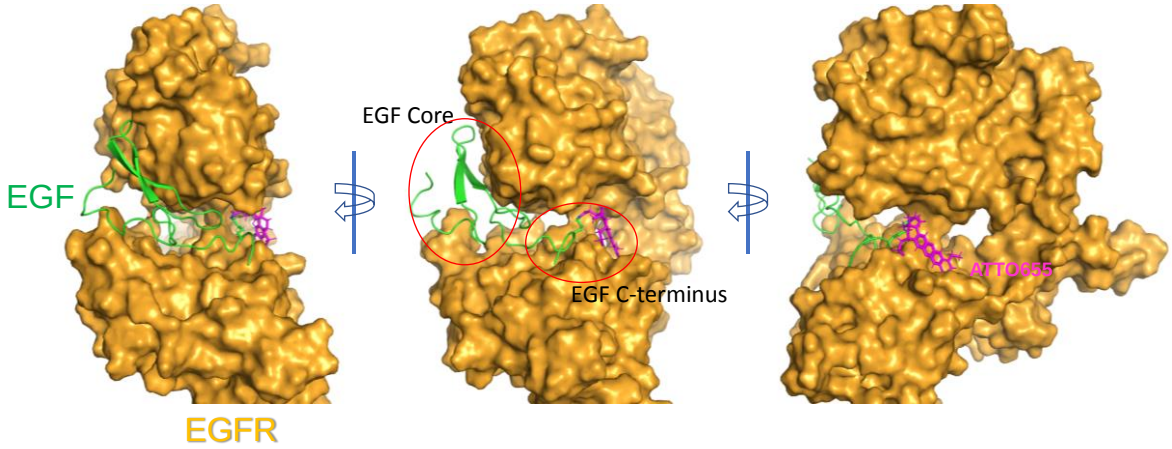

Figure S2. Structural prediction of the EGF-ATTO655/EGFR complex. The structurally rigid EGF core and the flexible C-terminal region are shown in red circles. The surface model represents the structure of EGFR and EGF is shown via the ribbon model. ATTO655 is drawn in magenta. Docking studies for the ATTO655-EGF-EGFR interaction were performed with previously reported EGF-EGFR structure (PDB entry, 1IVO) using Schrödinger program suite (Schrödinger, LLC, New York, USA). The Glide Covalent Docking was used for the prediction of ATTO655 conjugation to the K48 residue of EGF.

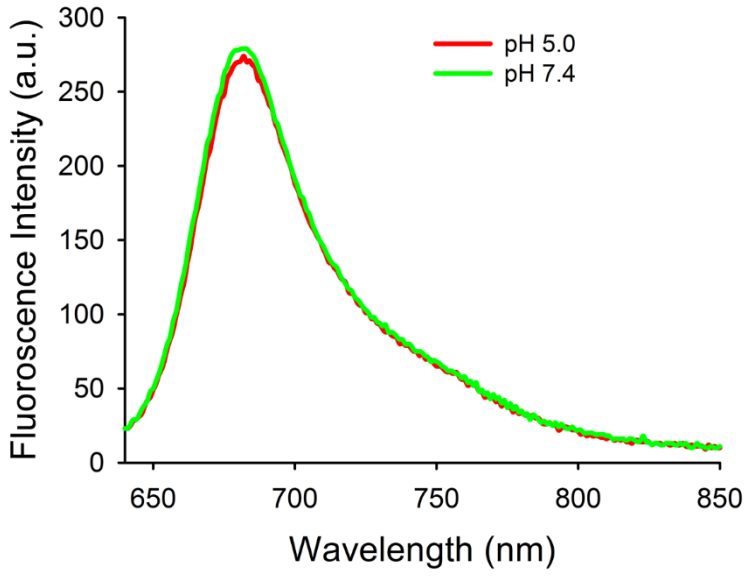

Figure S3. Representative fluorescence spectra of free ATTO655 dye at pH 7.4 and 5.0 conditions. Free ATTO655 dye (final concentration: 1 μM) was diluted with phosphate buffer solution (10 mM) at pH 7.4 and 5.0, and incubated for 17 h. Fluorescence spectra of the solutions (λ_{em} 600 nm, λ_{em} 610–850 nm) were measured every 1 h over a 17-h period using a multifunctional microplate reader. No difference in fluorescence intensities of the dye at pH conditions of 7.4 and 5.0 was observed over 17 h.

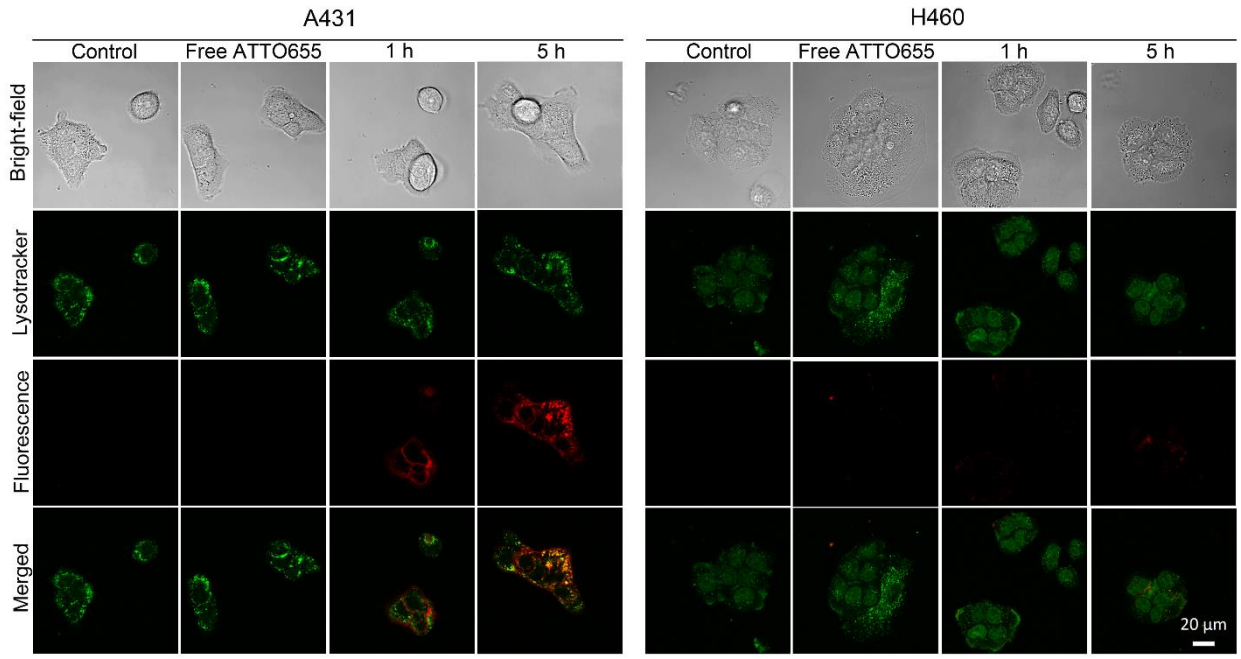

Figure S4. Confocal images of EGF-ATTO655-treated NCI-H460 (EGFR-negative) and A431 (EGFR-positive) cells. The cells were treated with free dye or EGF-ATTO655 for 1 and 5 h. After washing, cells were subjected to fluorescence microscopy analysis. For competition assay, A431 cells were pre-incubated with excess unlabeled EGF (+ EGF group) and then treated with EGF-ATTO655. Intracellular uptake of free dye (ATTO655) was also tested in both cell lines. Yellow regions indicate localization of EGF-ATTO655 at lysosomal sites.

Evaluation of EGFR-targeting specificity in various cell lines with different EGFR expression levels

NCI-H460, A431, HCC827 (human lung cancer cells, ATCC), and HCC70 (human breast cancer cells, ATCC) cells were seeded onto a 4-well Lab-Tek II chambered coverglass at a cell density of 50,000 cells per well and incubated overnight. The cell lines were incubated with EGF-ATTO655 (1 μM dye equivalent) for 5 h. After washing the cells thrice with cell culture medium, fluorescence imaging (λ_{ex} 633 nm, λ_{em} 638–759 nm) was performed using a confocal laser scanning microscope (Carl Zeiss LSM780).

For flow cytometry, cells from each cell line (1 x 10^5 cells/well) were seeded into 12-well plates for 24 h for cell attachment. Next, the cells were treated with cetuximab-Alexa647 conjugate (1 μM dye equivalent) for 10 min, and washed, and then, flow cytometry analysis was performed using LSRFortessa (λ_{ex} 640 nm, λ_{ex} 660/20 nm).

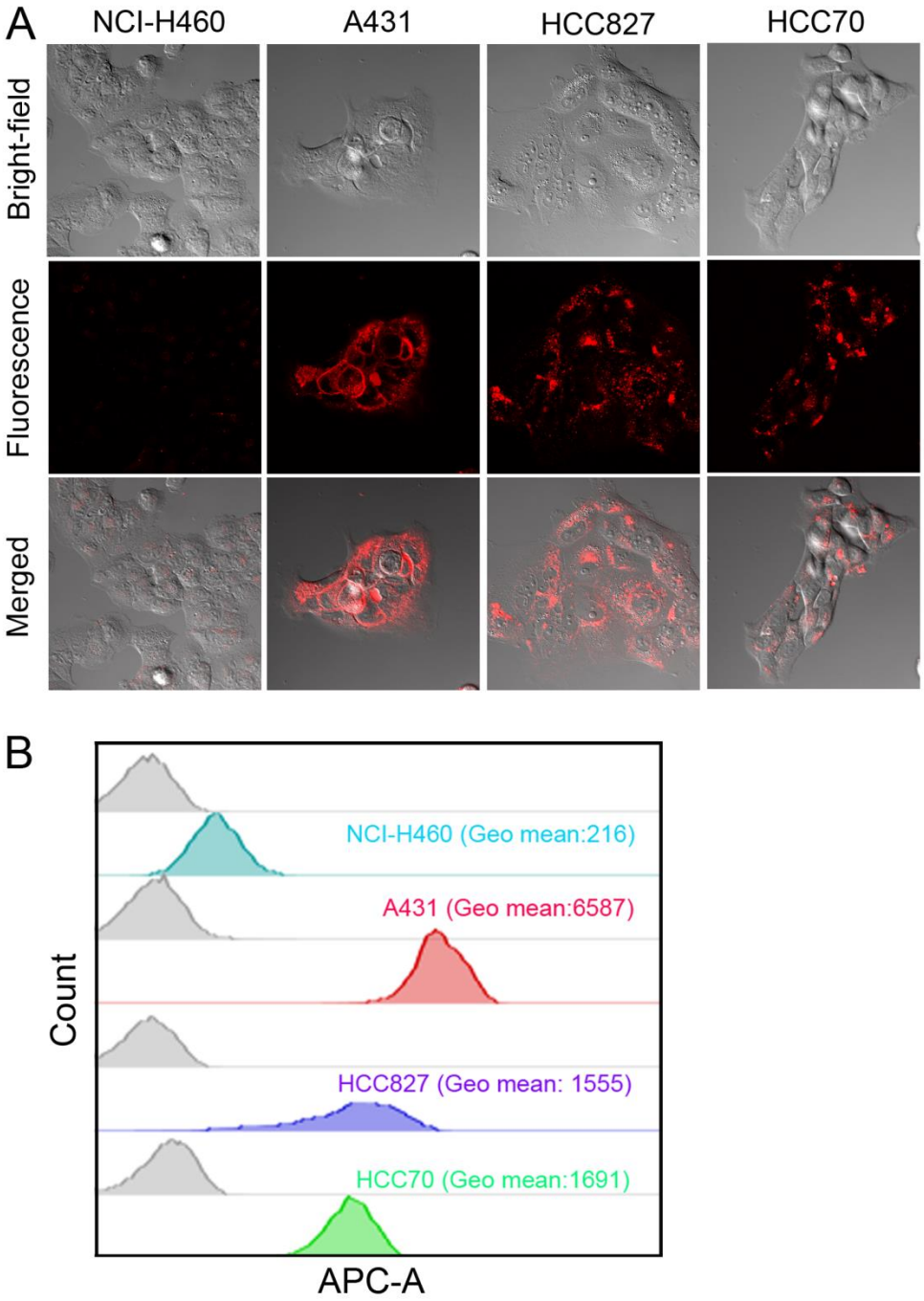

Figure S5. Evaluation of EGFR-targeted cellular uptake of EGF-ATTO655. A) Confocal images of EGF-ATTO655-treated NCI-H460 (low EGFR expression), A431 (high EGFR expression), HCC827 (moderate EGFR expression), and HCC70 (moderate EGFR expression) cells. These cancer cells were treated with EGF-ATTO655 (1 μM dye equivalent) for 5 h. After washing the cells, fluorescence images (λ_{ex} 633 nm, λ_{em} 638–759 nm) were obtained. B) Flow cytometry analysis of the EGFR expression levels in the tested cancer cell lines.

Synthesis and characterization of EGF-Alexa647

Human EGF (0.5 mg, 8 μmol) and Alexa647-NHS ester (8 μmol, Thermo Fischer Scientific Inc.) were dissolved in PBS solution (pH 7.4, 10 mM, NaCl, 137 mM; 0.5 mL) and allowed to react for 1 h at 25℃. The reaction mixture was passed through a PD-mini Trap G25 column to remove the byproducts and unbound dye. Next, the purified solution of the EGF-Alexs647 conjugates was concentrated using Amicon Ultra centrifugal filters and then stored at 4℃ until use.

To analyze the degree of labeling (i.e., number of conjugated dyes per an EGF), EGF-Alexs647 was diluted with PBS containing 1% SDS and 1 mM ME for the denaturation of the conjugate, and its absorbance at 650 nm was measured. The EGF concentration in the solution was calculated using the molar extinction coefficient of EGF (i.e., 18,825 $M^{-1}cm^{-1}$ at 280 nm). The degree of labeling was calculated to be 0.51.

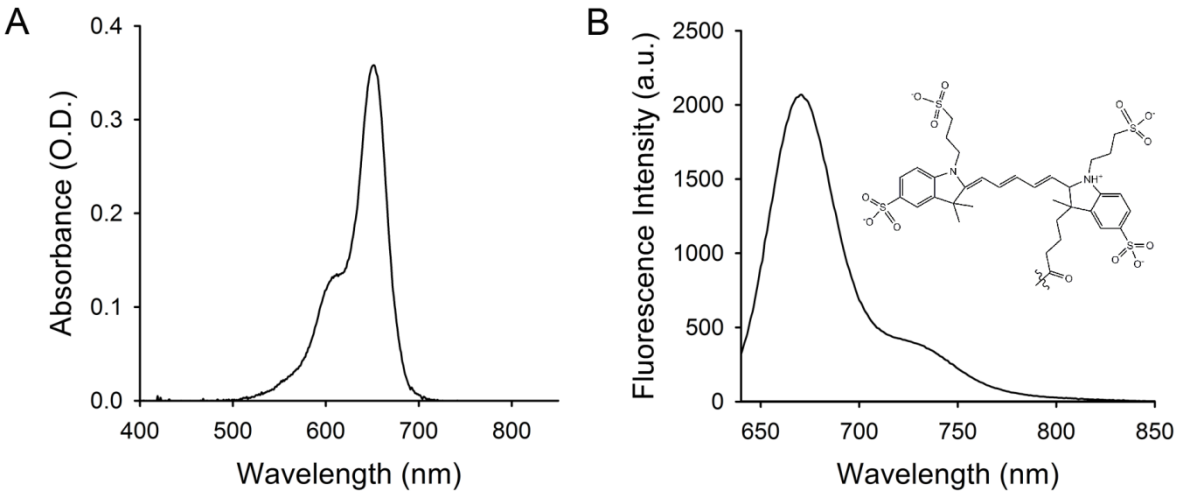

Figure S6. UV/Vis absorption (A) and fluorescence (B) spectra of EGF-Alexa647 in PBS buffer (5 μM dye equivalent). A stock solution of EGF-Alexa647 was diluted with PBS to the final concentration of 5 μM dye equivalent. Then, their absorption and fluorescence spectra were analyzed. Inset image: chemical structure of the conjugated Alexa647.

Real-time NIR fluorescence imaging of EGFR-positive cancer cells using EGF-Alexa647

EGFR-positive A431 cells were seeded onto a 4-well Lab-Tek II chambered coverglass at a cell density of 50,000 cells per well for real-time fluorescence imaging study. The cells were treated with EGF-Alexa647 at the concentration of 1 μM dye equivalent. NIR fluorescence images (λ_{ex} 640/30 nm, λ_{em} 690/50 nm) of the cells were obtained every 15 min without washing steps for 6 h using a Live Cell Imaging System (Carl Zeiss Axio observer Z1, EC Plan-Neofluar 10x/0.30 Ph1, Germany). After the completion of the live cell imaging, the cells were washed thrice with cell culture medium to remove the conjugates remaining in the extracellular space; then, fluorescence images of the cells were acquired once more. All the NIR fluorescence images were obtained using identical imaging settings.

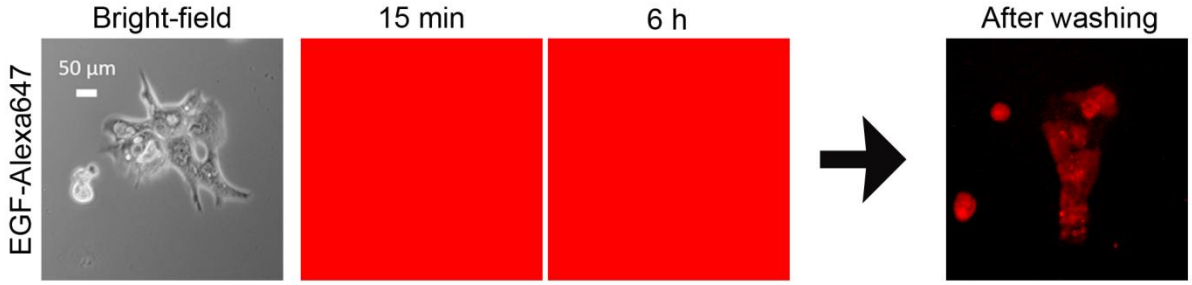

Figure S7. Real-time fluorescence imaging of EGF-Alexa647-treated A431 cells. After treating the cells with EGF-Alexa647 (1 μM dye equivalent), NIR fluorescence images (λ_{ex} 640/30 nm, λ_{em} 690/50 nm) were obtained every 15 min for 6 h without washing. Thereafter, the cells were washed, and then, fluorescence images were acquired once more.

Biodistribution of free dyes in normal mice

To compare the biodistribution of zwitterionic ATTO655 with negatively charged Alexa647, these dyes without EGF conjugation (50 μM, 100 μL/mouse) were injected intravenously via the tail vein. NIR fluorescence images of mice were obtained at 5 min, 1 h, and 3 h, and thereafter, the mice were scarified for the *ex vivo* imaging of their organs using the IVIS Lumina XR imaging system (λ_{ex} 620/20 nm, λ_{em} 670/40 nm).

We observed that most of the injected free ATTO655 dye was secreted through urine even before fluorescence imaging at 5 min post-injection. Therefore, only weak fluorescence signals were detected at 5 min and 1 h. In contrast, the urinary secretion of the injected Alexa647 was slower than that of ATTO655 dye. The *ex vivo* images of the organs indicate that the zwitterionic ATTO655 dye does not show nonspecific uptake in the liver, kidneys, and spleen.

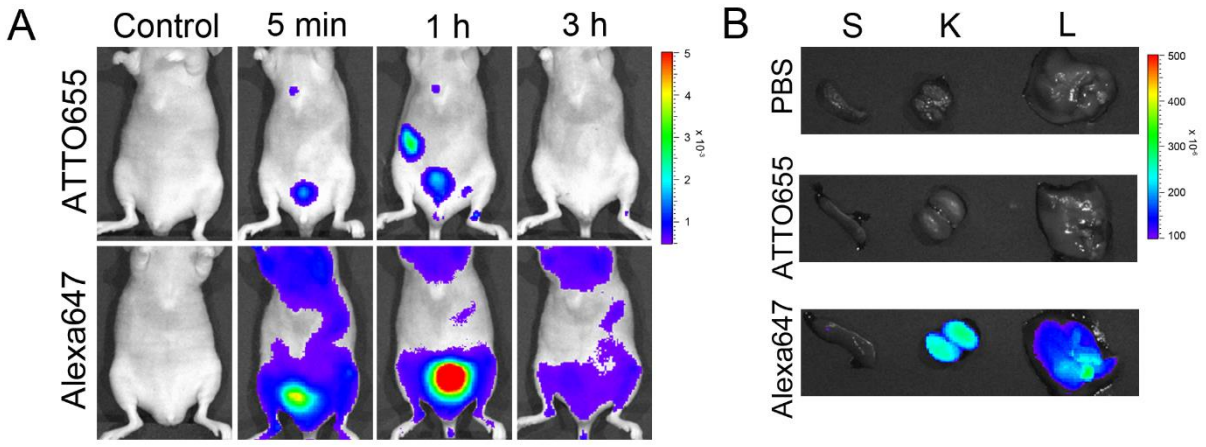

Figure. S8. Biodistribution of free dyes in normal mice. A) NIR fluorescence images of free ATTO655 and Alexa647 with time. B) *Ex vivo* imaging of the organs after 3 h (S: spleen, K: kidney, L: liver).

***In vivo* and *ex vivo* NIR fluorescence imaging of EGF-Alexa647**

A431 cells (5×10^6 cells/200 μL) were subcutaneously implanted into the right hind flank of each mouse (Balb/c-nu, female, 5 weeks age). When tumor sizes reached ~190 mm^3, the mice were subjected to an *in vivo* NIR fluorescence imaging study. The mice bearing EGFR-positive A431 tumors received intravenous injections of EGF-Alexa647 (n = 4, 100 μg/100 μL PBS/mouse). Then, NIR fluorescence imaging of the mice (λ_{ex} = 620/20 nm, λ_{em} = 670/40 nm) was carried out using the IVIS Lumina XR imaging system at 3 and 24 h post-injection. For the biodistribution analysis, the mice were sacrificed at 3 h and 24 h post-injection, and *ex vivo* NIR fluorescence imaging of the tumors and organs (kidneys, spleen, and the liver) were carried out. All the animal studies were approved by the Institutional Animal Care and Use Committee of National Cancer Center. The TBR values calculated at 3 and 24 h post-injection were 2.44 ± 0.13 and 2.25 ± 0.57, respectively. In particular, the mean fluorescence intensity from the kidneys was 4.85 times higher than that from the tumors. High fluorescence signals from the kidneys may be due to both high EGFR expression in liver and kidneys, and a high proportion of the renal elimination of the EGF conjugate [J. Nucl. Med. 2000; 41: 903-911].

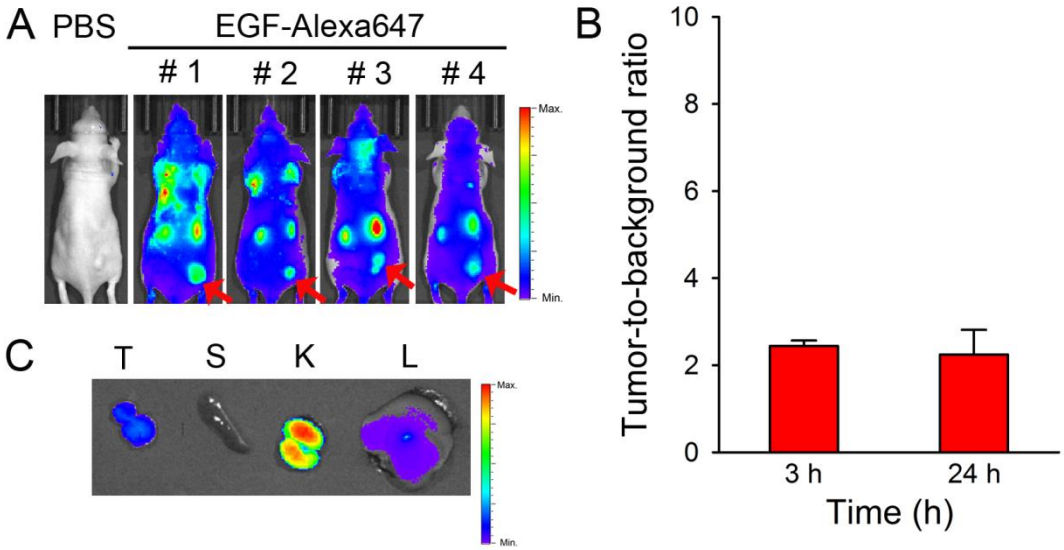

Figure. S9. *In vivo* NIR fluorescence imaging of EGF-Alexa647 in EGFR-positive A431 tumors. A) NIR fluorescence images of the mice bearing EGFR-positive A431 tumors at 3 h post-injection of EGF-Alexa647. The arrows indicate the tumor sites. B) Analysis of tumor-to-background ratio (TBR) at different time points (n=4). C) *Ex vivo* images of the tumor and other organs (T: tumor, S: spleen, K: kidney, L: liver) at 3 h post-injection are shown.